Received: 6 July 2022 | Revised: 20 September 2022 | Accepted: 2 October 2022

DOI: 10.1049/rpg2.12619

IET Renewable Power Generation

The Institution of Engineering and Technology WILEY

ORIGINAL RESEARCH

A hybrid method for day-ahead photovoltaic power forecasting based on generative adversarial network combined with convolutional autoencoder

Xueping Pan[1] | **Jieyang Zhou**[1] | **Xiaorong Sun**[1] | **Yang Cao**[1] | **Xiaomei Cheng**[2] | **Hossein Farahmand**[3]

[1]College of Energy and Electrical Engineering, HoHai University, Nanjing, China

[2]Department of Research and Development, Yara International, Oslo, Norway

[3]Department of Electric Power Engineering, Norwegian University of Science and Technology, Trondheim, Norway

Correspondence
Xueping Pan, College of Energy and Electrical Engineering, HoHai University, Nanjing, 210098, China.
Email: xueping_pan@hhu.edu.cn

Funding information
National Key Research and Development Program of China, Grant/Award Number: 2019YFE0105200

Abstract

Photovoltaic (PV) generation has high impact on the decarbonization pathways of power systems. Accuracy of day-ahead PV power forecasting has become crucial in the operation and control of power system with high PV penetration. This paper develops a hybrid approach based on generative adversarial network (GAN) combined with convolutional autoencoder (CAE) to improve PV power forecasting accuracy. Self-organizing map method is first utilized as data pre-processing to classify target days into different weather types based on solar irradiance. With the ability of GAN to reduce the burden of loss and the advantages of CAE to extract multi-scale effective features from the weather and PV power, PV power forecasting model consisting of GAN and CAE is proposed. The developed method has been tested on a real dataset in a Chinese PV station and compared with base reference PV forecasting methods. Numerical testing results demonstrate the effectiveness of our method with high accuracy.

1 | INTRODUCTION

Decarbonization of the energy sector plays an important role in mitigating the effects of climate change and global warming. In this respect, solar energy has been intensively investigated, given its positive contribution to the most pressing energy problems [1]. It is reported that in the first quarter of 2021, the installed capacity of photovoltaic (PV) in China has been increased by 5.33 million kW, and its cumulative installed capacity has reached 260 million kW [2].

High-level penetration of PV power generation to the electric grid leads to many technical challenges in the power grid stability and safety [3]. With the continuous expansion of the grid-connected PV systems, the precision of day-ahead PV power forecasting plays a crucial role in scheduling power production and procuring enough reserve capacity in power systems. Considering the variability and intermittency in PV production, the forecasting problems become even difficult.

In this paper, a hybrid method based on the generative adversarial network (GAN) combined with convolutional autoencoder (CAE) is developed for day-ahead PV power forecasting. The CAE is applied before the fully connected neural network in the generator of the GAN in the forecasting model. Its robustness and denoising ability based on spatial correlation extraction is utilized to improve the performance of PV power forecasting. The excellent performances of convolutional neural networks have directly contributed to the creation of CAEs. CAE is applied to dimensionality reduction and anomaly detection, which can handle two-dimensional spatial information well and improve the accuracy of input information. Combining CAE with the powerful unlabelled input data processing capability of GAN and the adversarial training process, the combination of the CAE and GAN can reduce the prediction error. The main contributions of this paper are summarized below

1. To analyze and extract different features of weather types, time series correlation analysis and the self-organizing map (SOM) method are applied. Weather types are clustered according to the ratio of diffuse horizontal irradiance (DHI) and global horizontal irradiance (GHI), and each type will

be forecast individually to capture the features of different weather types.
2. A hybrid method combining GAN with CAE is applied for the day-ahead PV power forecasting. The CAE is applied to dimensionality reduction and anomaly detection, which can improve the accuracy of input information. Combining this with the powerful unlabelled input data processing capability of GAN, the hybrid approach can reduce the prediction error.
3. Validation, testing and analysis of a real dataset in China as well as comprehensive comparisons with base references are conducted to demonstrate the efficiency and high precision of the developed method.

The rest of the paper is organized as follows. Section 2 summarizes and reviews the main methods for PV power forecasting. Section 3 illustrates the PV power data and relevant weather factors to investigate the features and extract the appreciate input for the forecasting model. The developed hybrid model of GAN combined with CAE is described in detail in Section 4. The numerical testing and analysis are provided in Section 5 followed by the concluding remarks in Section 6.

2 | LITERATURE REVIEW

The PV power forecasting methods have been variously investigated and analyzed [4–7] in recent decades. The most popular forecasting methods can be categorized into three types: the statistical time-series based methods, machine learning methods and the hybrid methods. A summarization of reviewed references and methods is presented in Table 1.

TABLE 1 List of reviewed forecasting methods

Statistical time-series methods	Linear regression	[8]
	Exponential smoothing	[9]
	Autoregressive moving average	[10]
	Autoregressive integrated moving average	[11]
Machine learning methods	Decision tree	[12]
	Support vector regression	[13]
	Artificial neural network	[14, 17, 18]
	RNN	[15]
	CNN	[20]
	LSTM	[19]
	Deep learning	[16, 21]
	DBN(deep belief networks)	[22]
	DCNN(deep convolutional neural network)	[23]
	AE, CAE	[24, 25]
	GAN	[26]
Hybrid methods	LSTM-RNN	[27]
	CNN-LSTM	[28, 29, 30]
	CAE-CNN	[31]
	CNN-GAN	[32]
	LSTM-GAN	[33]

2.1 | Statistical time-series-based methods

With the development of data mining technology, statistical methods based on historical data have been widely concerned in academia and industry. Time series provide statistical information to anticipate the characteristics of quantified elements and to predict the upcoming situation by evaluating past information [7]. The most popular statistical methods include simple linear regression [8], exponential smoothing [9], autoregressive moving average (ARMA) [10] and autoregressive integrated moving average (ARIMA) [11].

2.2 | Machine learning methods

Machine learning methods can learn from historical data and improve their predictive power through continuous iterative training, which can obtain the final prediction results through powerful training without predetermined formulas. The main methods of machine learning are decision tree [12], support vector regression [13], artificial neural network (ANN) [14], recurrent neural network (RNN) [15] and deep learning methods [16].

To capture the non-linear mapping between the input and output targets, ANN has been used in PV forecasting. Reference [17] compared the ANN model with three traditional mathematical schemes for PV output prediction and found that the ANN had much higher prediction accuracy. In [18], four different architectures of ANN are compared and it demonstrated high forecasting accuracy of ANN.

In the last few decades, ANN forecasting methods have been modified and developed, for instance, the RNN method with consideration of time correlation in data sequence, the long short-term memory (LSTM) method with super memory [19] and the CNN approach with strong ability to extract spatiotemporal correlation [20].

The non-linear processing capability of ANN facilitates PV power prediction, while the neural networks with shallow structure have the shortcomings of network instability and parameters non-convergence, which remain a problem that needs to be addressed, and the emergence of deep learning methods provides a good way to solve this problem [21].

Deep learning methods can learn from voluminous input data, use numerous hidden layers and better parameters to enhance the ability of forecast. A variety of research have concluded that application of deep learning methods in PV power forecasting has greatly improved the forecasting accuracy because of their strong feature extraction ability. The deep belief network (DBN) method has high-level abstraction extraction ability [22], the deep convolutional neural network (DCNN) approach can fit complex non-linear mappings and

processing different data sets [23], and the autoencoder (AE) approach have the characteristic of dimensionality reduction and denoising [24]. Furthermore, the encoding and decoding structure of CAE also has already demonstrated strong sky image prediction ability for spatiotemporal information in PV power forecasting [25].

Recently, a new deep learning model named GAN is proposed, which acts as a dominated approach in image synthesis and language processing. The GAN approaches, for example, the convolutional GANs and the conditional GANs, have been widely applied into different scenarios. For instance, the convolutional GAN performs outstandingly in PV power forecasting [26]. However, the small-scale timing information for detailed forecasting might be lost during the deep convolution process when high-frequency features are converted into low-frequency features.

2.3 | Hybrid methods

To incorporate different advantages of ANNs and to avoid their possible disadvantages, hybrid methods have been proposed and widely used recently in PV forecasting. In [27], a hybrid method with a combination of LSTM-RNN was proposed for PV power forecasting, and the coupling between weather and electricity was incorporated into the forecasting model, the proposed hybrid method had shown better performance than individual LSTM and RNN. In [28], the authors proposed a novel multivariate hybrid deep neural model named WPD-CNN-LSTM-MLP for 1-h-ahead solar irradiance forecasting. In [29, 30], two hybrids of CNN-LSTM and ConvLSTM were applied and the PV forecasting results show better forecasting accuracy than a normal LSTM model. Besides, in the hybrid of CAE and CNN, the CAE method can enhance the network depth and widen the network through establishing long skip connections in deep CNN [31]. In [32], the method of using GAN to enhance the training dataset and then training by CNN not only improves the accuracy of prediction but also has high efficiency compared with traditional methods. Meanwhile, the generator of GAN can be substituted with LSTM structures to avoid the mean trap in time series forecasting. However, with multiple input variables consideration, spatial correlations extracted through convolutions by CNN have better performance than temporal correlations extracted by LSTM in PV power forecasting [33]. Compared with CNN, CAE has stronger feature extraction and de-noising ability, and the combination of CAE and GAN may produce better predictions.

3 | PV POWER AND AFFECTING VARIABLE ANALYSIS

PV power data and relevant weather factors are analysed in this section to dig into the time series correlations and characteristics, and the appropriate input for the forecasting model is selected.

3.1 | Data analysis

To analyse the features of PV power and weather data, one PV power dataset from a regional PV station with 25-MW rated power in Jiangsu Province, China is investigated. The station faces south, with a tilt angle of 29°. The PV power data is collected from 1 January, 2017 to 31 December, 2017 from 5 AM to 7 PM in step of 5 min. The corresponding meteorological data is collected from the numerical weather prediction (NWP) by climate database Solargis v2.1.21 (https://solargis.com/cn). The weather variables collected include GHI, DHI, global tilted irradiance (GTI), temperature (TEMP), wind speed (WS), and wind direction (WD).

Scatter plots of the weather data versus PV power are shown in Figure 1. As can be seen, approximate linear relationships exist between the PV power and weather factors of GHI and GTI. Weather factors DHI, TEMP, and WS have highly nonlinear patterns with the PV power, while WD is almost irrelevant with the PV power. The scatter plot indicates non-linear forecasting methods are necessary to capture the high non-linear features among PV power and weather variables.

Time series autocorrelation analysis is also conducted for the six weather variables, as shown in Figure 2. It can be seen that the PV power to be estimated has a strong correlation not only with the adjacent values, but also with distant values of the input data. Therefore, the local reception characteristics of traditional ANN or CNN may lose importance features in the input variables. Forecasting methods consisting of fully connected network or hybrid methods would be thus suitable for forecasting problems in view of their ability in keeping all features of the input data.

3.2 | Model input selection

The Pearson correlation coefficient is used to investigate linear correlations among time series $\{x\}$ and $\{y\}$:

$$\rho_{xy} = \frac{\sum_{t=1}^{n} (x_t - \bar{X}) \times (y_t - \bar{Y})}{\sqrt{\sum_{t=1}^{n} (x_t - \bar{X})} \times \sqrt{\sum_{t=1}^{n} (y_t - \bar{Y})}} \quad (1)$$

where n is the length of time series, $\bar{X}$ and $\bar{Y}$ are the average of two time series, respectively. The parameter $\rho_{xy} \in [-1,1]$ is the correlation coefficient of two time series.

The Pearson correlation results between the collected historical PV power and six weather variables are shown in Figure 3. It can be seen from Figure 3 that GHI, DHI and GTI have high correlations with PV power, and this indicates that solar radiation makes great contribution to the PV power output. In addition, the correlations between TEMP, WS and PV power are relatively high, with the value of 0.303 and 0.242, respectively. This implies the positive impacts of TEMP and WS on PV power production. Furthermore, it can find that WD has a very low influence on the PV power production according to the lowest correlation between WD and PV (with the value

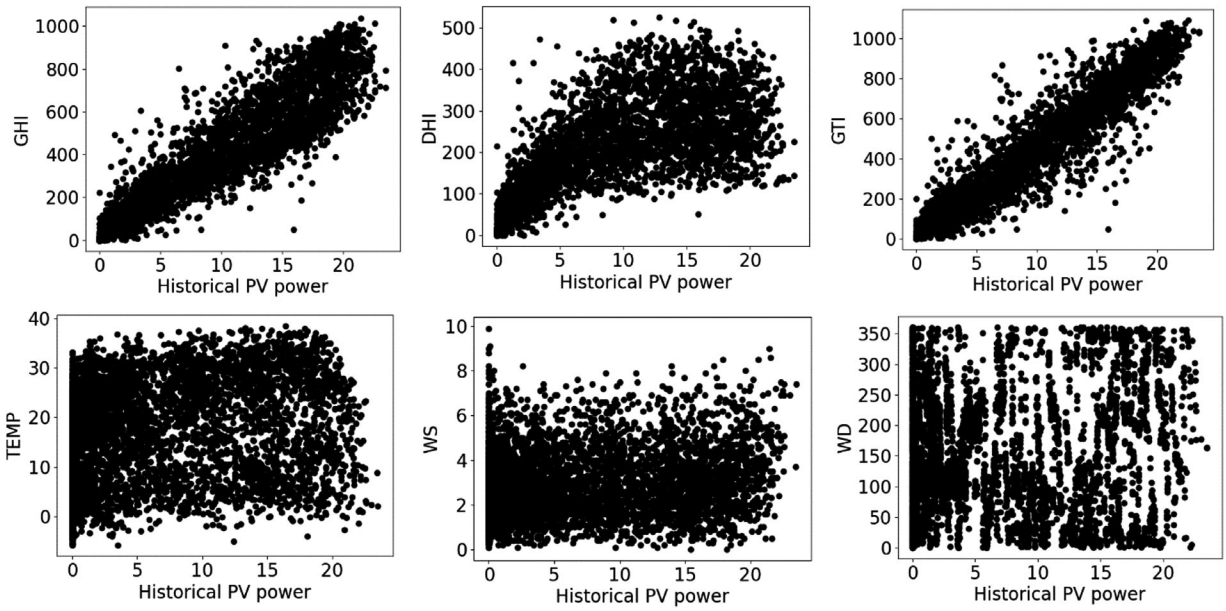

FIGURE 1 Scatter plots of weather variables versus PV output

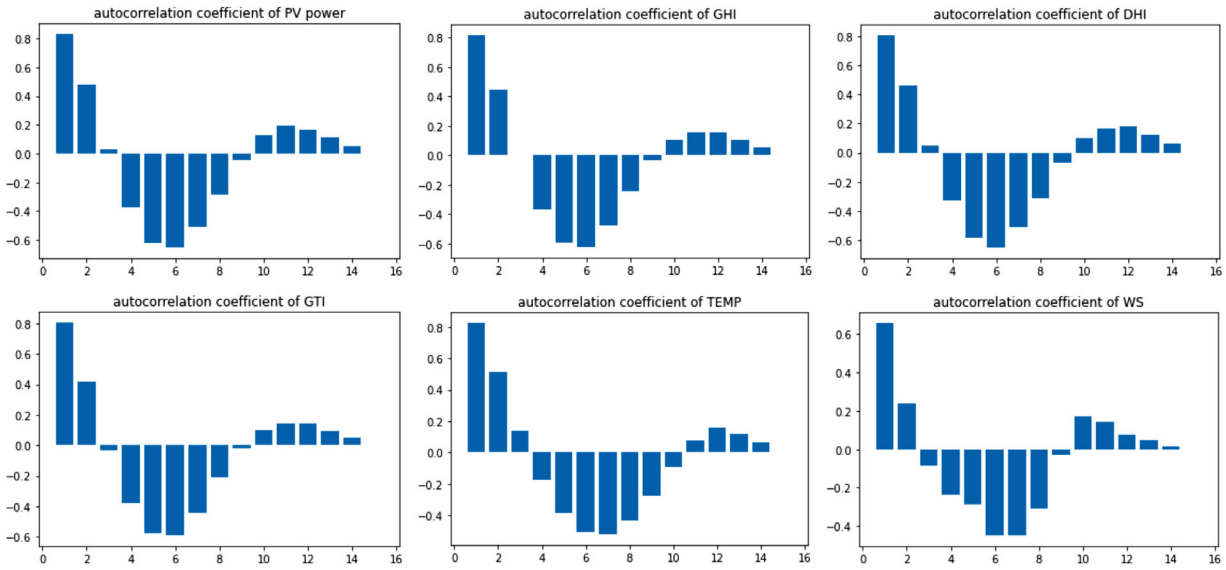

FIGURE 2 The autocorrelation results of the six input variables

of 0.00412). This means that WD can be removed from the dataset. Therefore, the five weather variables (GHI, DHI, GTI, TEMP and WS) with coefficient above 0.2 and historical PV power are chosen as the input factors for the day-ahead PV power forecasting. Selection criteria and threshold may vary with different testing cases.

4 | METHODOLOGY

This section presents the forecasting methodology. Architecture of the developed method is depicted in Figure 4. The data pre-processing block focuses on clustering the weather types according to the ratio of DHI and GHI. All weather data are categorized into three parts corresponding to the sunny days, cloudy day and rainy days. Individual forecasting model GAN combined with CAE is then developed and applied to forecast the PV power for each weather type data.

4.1 | SOM-based clustering

Data pre-processing is the first and mandatory step to conduct the feature extraction for PV power forecasting. Many different

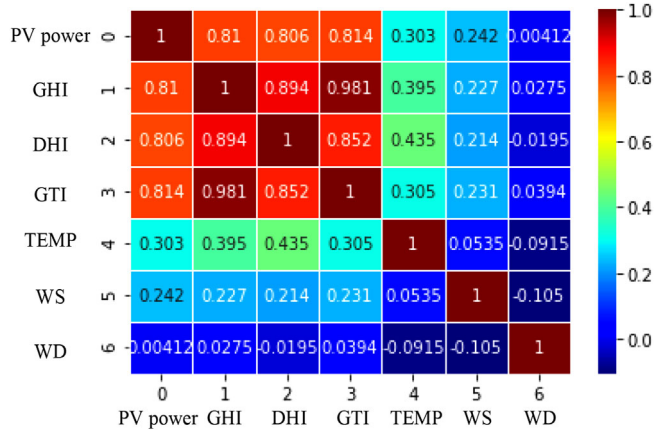

FIGURE 3 Pearson correlation coefficient between meteorological variables and PV power

approaches have been used in data pre-processing. However, the clustering technologies highly depend on prior information to obtain the number of target clusters [34]. The approach of SOM neural network developed in [35] is a special type of neural network used in clustering, which does not require prior information or complicated formula and is less affected by noisy data [36]. Therefore, correlation analysis and the SOM neural network are applied for data pre-processing in this research.

According to the national standard formulated by China Meteorological Administration, weather statuses (i.e. atmospheric conditions) are divided into 33 weather types [37]. Among all these weather types, sunny, cloudy and rainy are the three typical types occupying the majority of weather statuses. To reduce the complexity of classification, and to have reasonable historical data of weather types with low occurrence frequency, three typical weather types of sunny, cloudy and rainy are considered in this paper.

Three typical weather types are clustered by the SOM neural network method before feeding into the forecasting engine. Clustering process of the SOM method is illustrated in Figure 5. It consists of two layers including input layer and competitive layer. The mean and standard deviation of the daily total DHI and GHI ratio for each weather type are the inputs [38], which are transformed by the SOM neural network into a two-dimensional map of features in a topological-ordered fashion in the input layer. In the competitive layer, the neurons are classified into different reaction zones through self-organizing learning. Hence, the input could be automatically classified.

4.2 | Input data formulation

According to the local sunrise and sunset in different seasons, including the extreme conditions in both winter days and summer days, the PV power generation of the selected PV station generally happens from 5 AM to 7 PM (time zone: GMT + 8). For simplicity, we thus consider the consistent solar hours from 5 AM to 7 PM throughout the day. The input data to the generator of GAN is conducted as a two-dimensional matrix with six rows (corresponding to six variables including five weather variables and historical PV power) and 15 columns (corresponding to 15 hourly spans from 5 AM to 7 PM), which is shown in Figure 6. The input matrix can be treated as a two-dimensional pixel map, of which the inner spatial correlation is convenient for CNN to extract. Similarly, the input data to the discriminator of GAN is also a two-dimensional map constructed from the PV power time series of the predicted day.

4.3 | The model of GAN combined with CAE

Structure of CAE GAN is illustrated in the bottom red box of Figure 4. The GAN consists of two networks: the generator network and the discriminator network. The two-dimensional historical PV power and five weather variables are the input of the generator network, while the output of the generator network is the predicted PV power *f*. The discriminator network works as a classifier, which aims to discriminate the predicted power *f* from the actual PV power *y*. The adversarial GAN loss promotes the generator network to calculate an accurate predicted value that approximates the distribution of the actual value. After the training, the generator network of GAN will be adopted for PV power prediction.

The CAE is implemented before fully connected neural networks in the generator of GAN to capture the inner feature between input data (including historical PV power and five weather variables) and the actual PV power of the forecasted day. The CAE works as a symmetrical U-shaped connected convolution network, which contains two parts. The first encoder part is used to extract low-frequency features and their interaction relationships from the input variables while the second decoder part enables precise localization using up-convolutions and reconstructs the denoised and effective feature map. As shown in Figure 4, the encoder consists of a series of blue boxes corresponding to the multi-channel feature map. The number of channels denoted on the top of the box represents the number of convolution kernels in the last convolution process. The decoder part consists of stacked blocks, which is similar to those of the encoder. Furthermore, up-convolutions (green arrow in Figure 4) are added between each two decoding blocks. Therefore, the feature maps from different layers can be unified in size and concatenated together. In addition, the encoder and decoder parts are concatenated through long jump connections, which provide different-level features for more contact information until the output map fuses effective features of all layers. The schematic of convolution and up-convolution is shown in Figure 7.

The discriminator network of GAN plays an adversarial role to support the generator network to predict accurate PV power. In this research, the CNN, which is based on classic LeNet architecture [39], is used for the discriminator network. The CNN comprises fully connected layers, convolutional layers and two non-linear activation functions: Leaky_Relu and Sigmoid. The main objective of the convolutional layer is to extract deep low-resolution features for accurate classification of actual values and predictions, while the fully connected layer

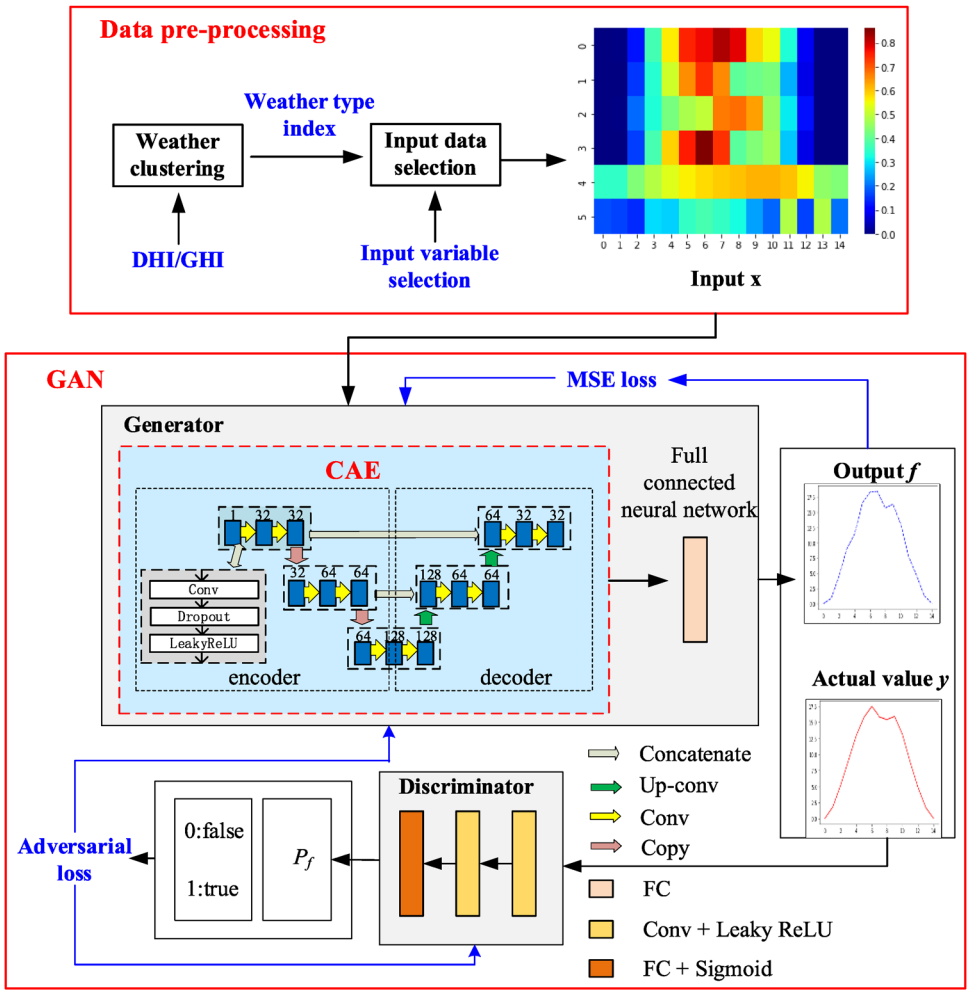

FIGURE 4 Architecture of the developed forecasting method

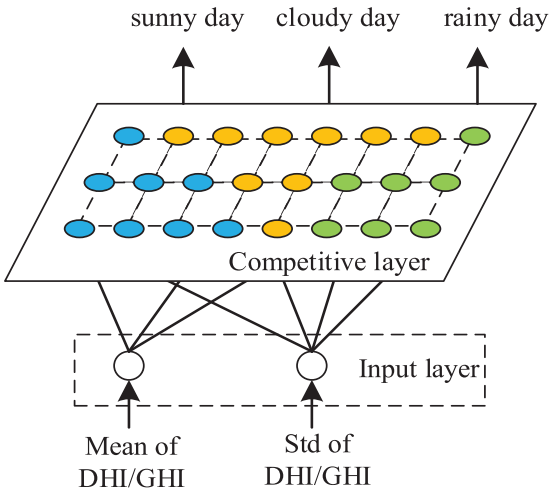

FIGURE 5 Schematic of SOM

linearly combines pixels of the feature map to a vector. The non-linear activation functions are to investigate the non-linear relationships.

In GAN, the objective of the generator network is to analyze the mapping from the input x to the actual data y, which can be expressed as: $G : R^x \rightarrow R^y$. The main purpose of the discriminator is to distinguish the prediction f from the actual value y based on supervised {0, 1} classification, which can be represented as $D : R^f \times R^y \rightarrow \{0, 1\}$. In adversarial training, the discriminator D attempts to distinguish generator G's outputs f from the actual data y with 'fake' and 'real' labels while generator G aims to predict accurately and fools D to obtain 'real' labels. The training of GAN is a two-player minimax game, and the objective function is as follows [26, 40].

$$\begin{aligned}&\min_G \max_D V(G,D)\\&= \min_G \max_D \left\{E_y[\log D(y)] + E_x[\log(1 - D(G(x)))]\right\}\\&= \min_G \max_D \left\{\frac{1}{m}\sum_{i=1}^{m} \log D(y^i) + \frac{1}{m}\sum_{i=1}^{m} \log\left[1 - D(G(x^i))\right]\right\}\end{aligned} \tag{2}$$

where V is the training objective of GAN, E stands for averaging, m is the data number, $D(y)$ is the possibility of actual sample

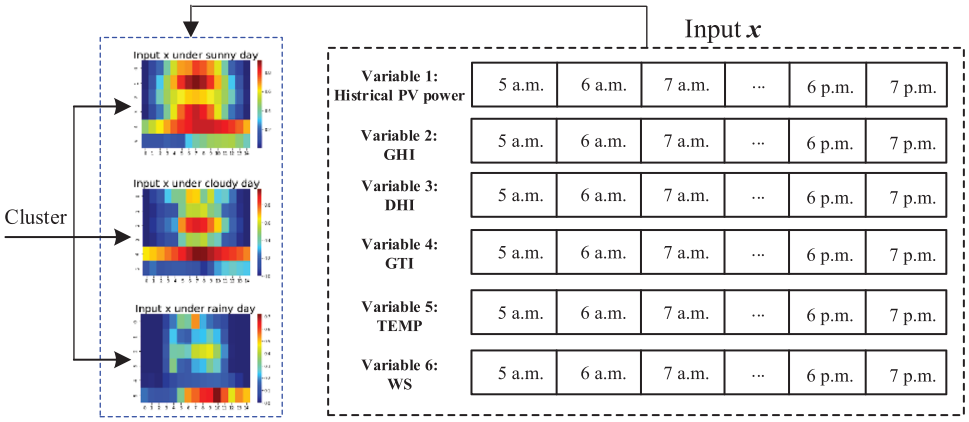

FIGURE 6 Two-dimensional input data

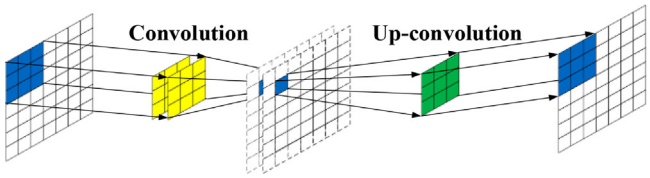

FIGURE 7 Schematic of convolution and up-convolution

y belonging to actual data and $D(G(x))$ is the possibility that the predicted sample $G(x)$ belongs to the actual data. During the training process, G tries to minimize the objective against an adversarial D which tries to maximize it. When $D(y)$ is close to 1 and $D(G(x))$ is close to 0, $V(G, D)$ can be large enough. On the contrary, when $D(G(x))$ is close to 1, $V(G, D)$ will be very small. The optimal solution of both G and D can be achieved when their confrontation reaches the Nash equilibrium.

References [40] and [41] have shown that mixing the adversarial loss with traditional loss, such as MSE loss, can speed up the convergence through facilitating the predicted values f close to the actual values y from the point-to-point value. In this paper, the MSE loss is defined as follows:

$$L_{MSE} = \frac{1}{n}\sum_{t=1}^{n}(y_t - f_t)^2 \tag{3}$$

where n is the length of input time series, y is the actual output time series, f is the output of the GAN generator.

Consequently, the ultimate training objective of the generator can be described as

$$L_G = (1-\lambda)\min_G \max_D V(G, D) + \lambda \min L_{MSE}(G) \tag{4}$$

where λ is the weight coefficient.

Flow chart of the above developed PV power forecasting method is illustrated in Figure 8 with detailed steps as follows:

Step 1: Five weather variables (GHI, DHI, GTI, TEMP and WS) are selected as input variables according to the correlation analysis between PV power generation and the weather variables.

Step 2: Based on the ratio of DHI and GHI, weather types are clustered into three categories, that is, sunny, cloudy and rainy day by SOM neural network.

Step 3: Two-dimensional data with time series as horizontal coordinate and the historical PV power and weather data as longitude coordinate is constructed as input to GAN's generator.

Step 4: Feature extraction is attained based on CAE. The encoder extracts the deep features of the two-dimensional input data, and the multiple frequency effective features from different layers are fused in the decoder part of CAE.

Step 5: The fully connected neural network in the generator of GAN linearly transforms the output map from CAE into the time series of PV power.

Step 6: The discriminator of GAN with the range [0,1] works as a classifier to distinguish the predicted value of PV power from the actual value. The higher the output of discriminator, the closer between the predicted value and the actual power.

Step 7: Calculation of the adversarial loss and MSE loss.

Step 8: When the mixture of adversarial loss and MSE loss reaches the end of the epoch, the training ends and the PV power time series output by the generator of GAN are the forecasted values. Otherwise, the parameters of GAN are continuously updated based on the gradient feedback and correction and return to step 4 for the next training iteration.

5 | CASE STUDY

The regional PV station with 25-MW rated power in Jiangsu Province, China, is investigated for the testing and analysis. In the following, weather type clustering, model parameter tuning, the performance of the developed method and the comparison with other popular methods are presented.

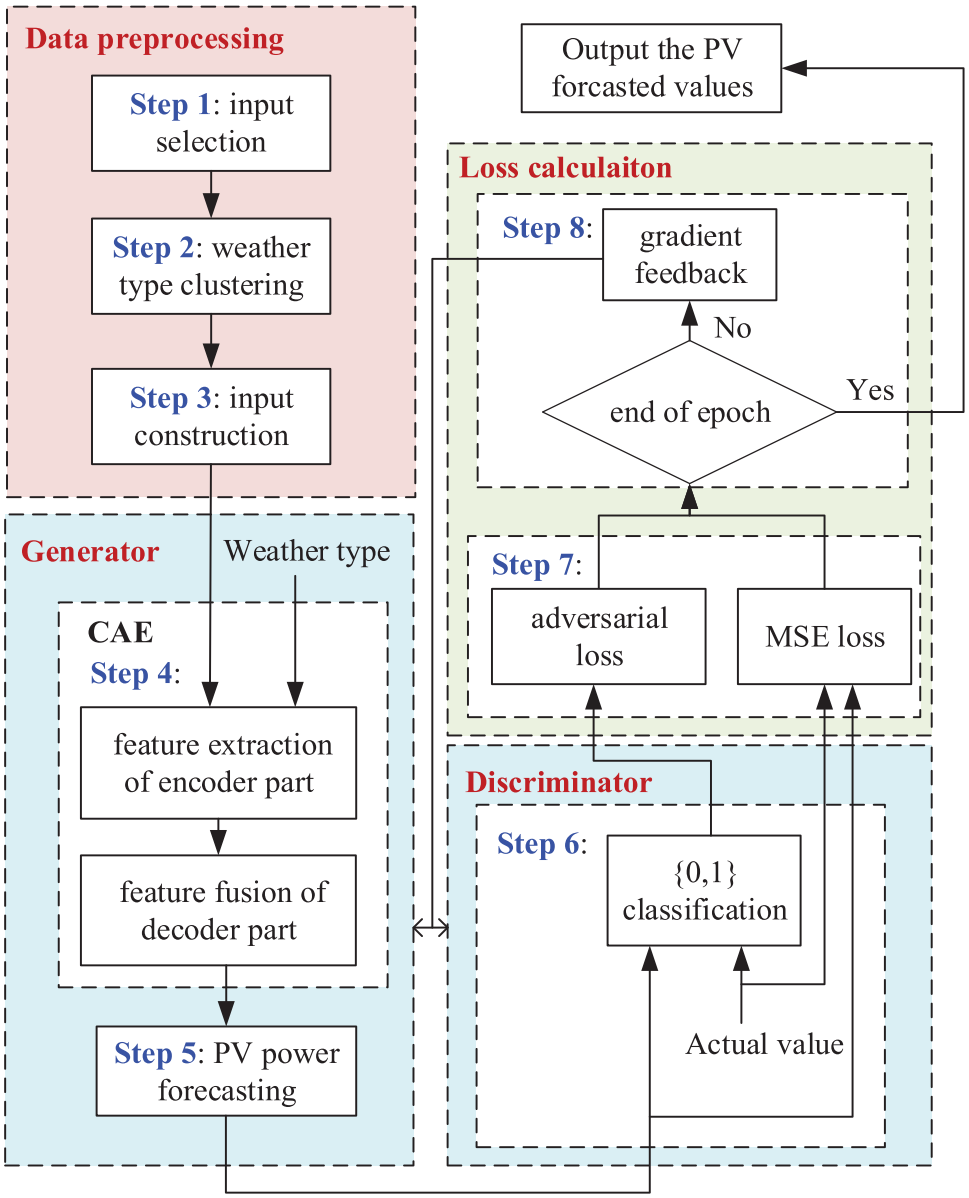

FIGURE 8 Flow chart of the developed PV forecasting approach

The PV power forecasting structure has been implemented in Python 3.6, and tested on a 64-bit i9-10900 CPU 16G RAM personal computer. Training and testing the model are based on Pytorch 1.5.0 deep learning framework. The forecasting performance is evaluated using three criteria: mean absolute error (MAE), MAPE and RMSE:

$$MAE = \frac{1}{n}\sum_{t=1}^{n}|y_t - f_t| \tag{5}$$

$$MAPE = \frac{1}{n}\sum_{t=1}^{n}|y_t - f_t| \Big/ \frac{1}{n}\sum_{t=1}^{n} y_t \times 100\% \tag{6}$$

$$RMSE = \sqrt{\frac{1}{n}\sum_{t=1}^{n}(y_t - f_t)^2} \Big/ \frac{1}{n}\sum_{t=1}^{n} y_t \times 100\% \tag{7}$$

where f and y are the predicted time series and actual time series of PV power generation, respectively.

5.1 | Weather type clustering results

As discussed in Section 4.1, weather types are summarized as sunny, cloudy and rainy days. To improve the performance of the weather type clustering, 5-min interval historical PV power and weather data is investigated. Figure 9 shows the typical PV power curves from 5 AM to 7 PM of three weather types.

Both DHI and GHI are solar irradiance at horizontal direction, and DNI is the direct normal irradiance. The GHI equals DHI+DNI*cosθ with θ as the zenith angle. Since DNI is large at sunny days, the ratio of DHI/GHI is thus be small. On

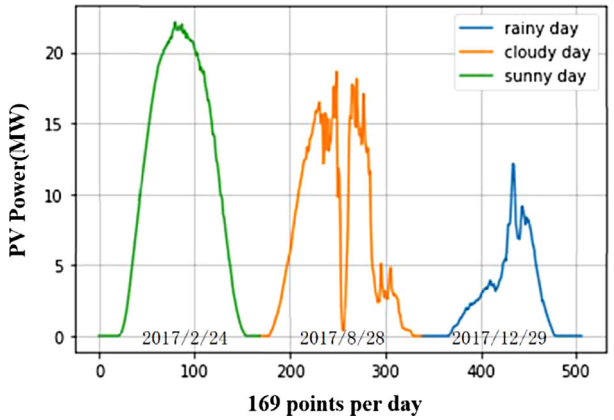

FIGURE 9 Typical power curves of different weather types

TABLE 2 Clusters of weather types according to DHI/GHI

Number of days	Weather cluster	Range of $\frac{\sum_{i=1}^{n} \mathrm{DHI}(i)}{\sum_{i=1}^{n} \mathrm{GHI}(i)}$
134	Sunny day	[0, 0.532)
141	Cloudy day	[0.532, 0.803)
90	Rainy day	[0.803, 1]

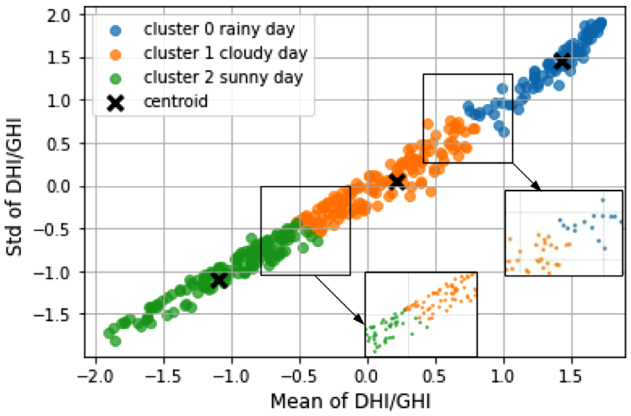

FIGURE 10 Weather type clustering results of the regional PV station

the contrary, DNI is small at rainy days, and the ratio of DHI and GHI is thus large. Based on the ratio of DHI and GHI, weather clustering results by SOM neural network are presented in Table 2 and Figure 10. It can be seen that the clusters are centrally distributed, and the boundaries of each cluster are relatively clear. The number of sunny days, cloudy days and rainy days is 134, 141 and 90, respectively. The range of DHI/GHI is [0, 0.532] at sunny days, [0.532, 0.803) at cloudy days and [0.803, 1] at rainy days.

5.2 | Training parameter setting

In this paper, considering the depth of map, both the input and the output data of CAE are constructed as three-dimensional

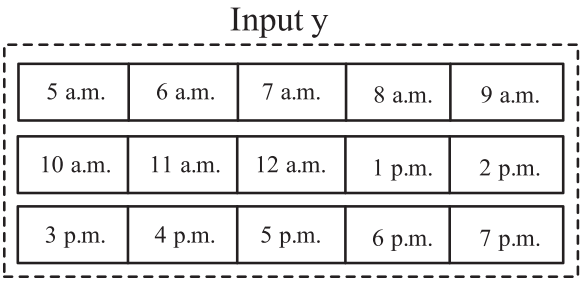

FIGURE 11 The three-dimensional map of internal use of the input data for GAN discriminator

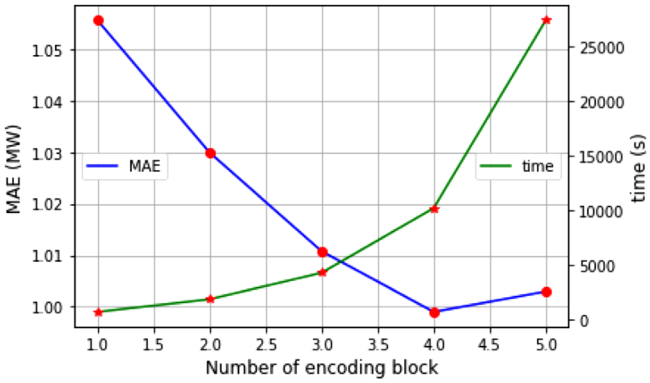

FIGURE 12 Effect of network depth on MAE and training time

structures with 1 depth, 6 rows and 15 columns (abbreviated as 1 × 6 × 15), and the output data of the generator in GAN is PV power time series with a two-dimensional structure 1 × 15. The input data of the discriminator in GAN is the actual power of the PV station and has the same dimension with the output of the GAN generator, which is one dimension as 15. To achieve the efficiency of convolution neural networks, the internal use of GAN discriminator is 1 × 3 × 5 three-dimensional map shown in Figure 11 through a sequential listing of the PV power time series, and the output of the discriminator indicates the probability that the input PV power follows the distribution of actual ones.

Other parameters in the model of GAN combined with CAE are presented in Table 3. To avoid the compatibility and adaptability problem caused by the length and width change of the feature map during convolution processes, the length and width of the map are set to be constant. Therefore, the padding of convolution is generally set to half of the kernel size, and the stride of convolution is set to 1.

The forecasting performance with different CAE depths is shown in Figure 12. It can be seen that when the number of encoder blocks exceeds 3, the MAE is less than 1.01. However, the computation time will experience twofold increase. Therefore, three encoder blocks are selected in this paper. In the future, we will further consider to improve the CAE efficiency with less computational time.

Other hyperparameters are determined through the validation process. During the training process, the generator and discriminator are updated with a consistent learning rate of

TABLE 3 The network parameters of GAN

Compositions				Parameters
GAN Generator	CAE	Encoder part	Convolution	Number of kernels: 32/64/128 Size of kernels: 3 × 3
			Dropout	Dropout rate: 0.5
			Leaky_Relu	Negative slope: 0.2
		Decoder part	Up-convolution	Number of kernels: 64/32 Size of kernels: 1 × 1
			Convolution	Number of kernels: 64/32 Size of kernels: 3 × 3
			Leaky_Relu	Negative slope: 0.2
	Full Connection Network		FC	Number of nodes: 15
			Leaky_Relu	Negative slope: 0.2
GAN Discriminator	Convolution			Number of kernels: 64/32 Size of kernels: 3 × 3
	Leaky_Relu			Negative slope: 0.2
	FC			Number of nodes: 1
	Sigmoid			–

0.00015, and the gradient correction and network parameter optimization are carried out by Adam algorithm. As for the weighting coefficient of the adversarial loss and MSE loss, the value of λ is set to 0.9. Depending on the complexity of testing cases, the termination of the iterations in the training can be set as number of epochs or targeted training error. For this study case, the number of epochs of the iterations is used, and the value is set as 300.

5.3 | PV power forecasting based on GAN combined with CAE

The 365-day dataset is first categorized into three parts based on SOM clustering results. For each cluster, the number of sunny days, cloudy days and rainy days is 134, 141 and 90, respectively. Data of each weather type are then further divided in three sets through three-way data split, that is, for each weather type dataset, there are a training set (70%), a validation set (20%) and a testing set (10%). Thus, each weather type is individually forecasted within its own three-way data split dataset. The model of GAN combined with CAE is trained based on the training and validation dataset, and then PV power is forecasted with the testing data.

The total 73-day testing dataset consists of 27 sunny days, 28 cloudy days and 18 rainy days. Figure 13 depicts the box plot of hourly PV power forecasting MAE for the 73-day testing data. The red line, the green triangle mark and the black cycle represent the median, the mean value and the outliers, respectively.

It can be found from Figure 13 that

1. The highest forecasting error happens on cloudy days, followed by rainy days and the lowest on sunny days. Although fully adaptive clustering does not require prior knowledge, the boundary between cloudy days and sunny days might be blurred, as shown in Figure 10. This may result in a mixed cluster of a cloudy day and a slightly higher MAE for cloudy days than rainy days.
2. The highest forecasting error happens between 12:00 and 13:00 during the day. It indicates that the PV power, when solar radiation turns from vertical to decline, is the most challenging period to predict.

After eliminating outliers in Figure 14, the 90%, 80% and 70% confidence intervals of the PV power forecasting MAE are shown in Figure 14. The blue dot and the green line represent the scatter of MAE and the mean of MAE, respectively. The blue, purple and orange areas represent the 90%, the 80% and the 70% confidence interval, respectively.

It can be found that the MAE volatility decreases with the decrease of the confidence interval. On sunny day, the MAE is typically low except for at 14:00, and the MAE distribution is relatively uniform at each time. There are high MAE fluctuations between adjacent times on cloudy and rainy days, the multi-peak trend in the MAE distribution can be explained by the weather uncertainties. The maximum MAEs tend to be happened at 12:00 for both on cloudy and rainy days.

Cross-validation is often not used for evaluating deep learning models because of the great computational expense. However, it could help when the dataset is not sufficient. In the following, cross validation for the rainy day PV power forecasting is applied since the number of rainy day is the smallest among three weather types.

The 90 rainy days are split into 10 folds, in which 63 days (70%) of data are used for training, 18 days (20%) of data are used for validation and 9 days (10%) of data are for testing.

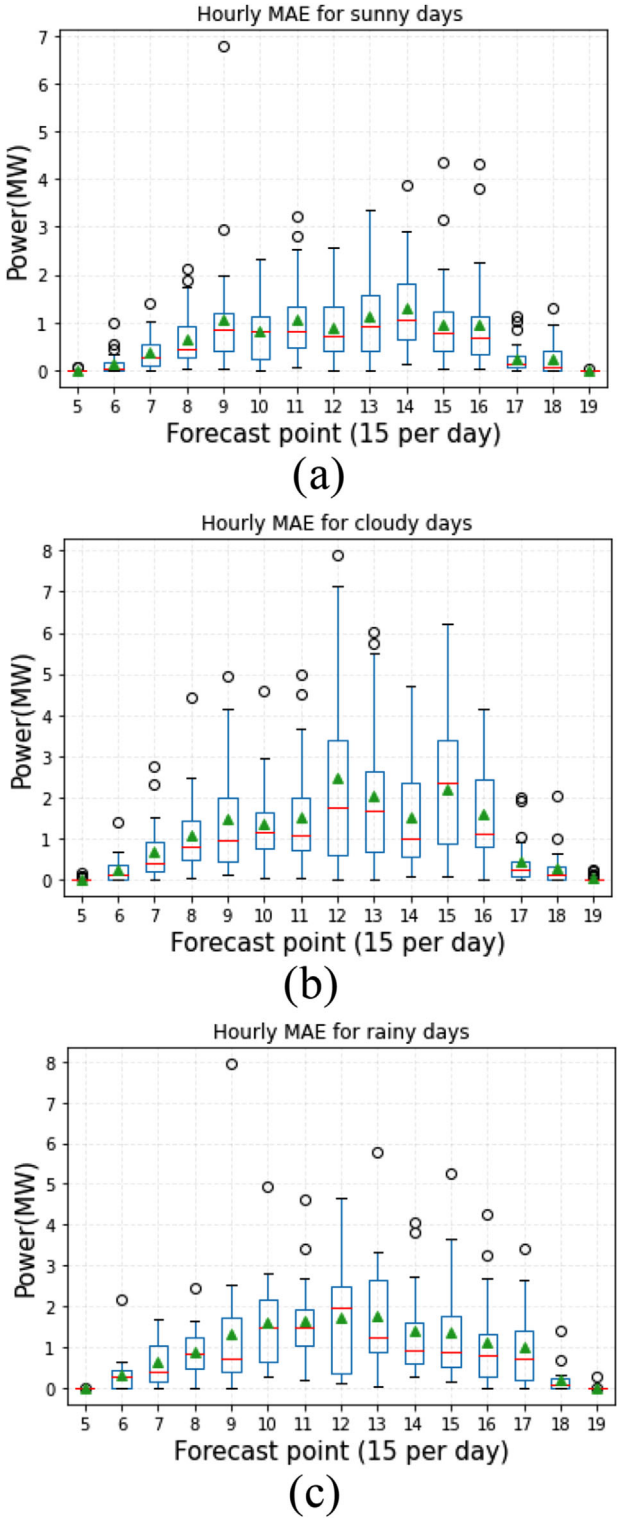

FIGURE 13 Box plot of hourly MAE: (a) sunny day, (b) cloudy day, (c) rainy day

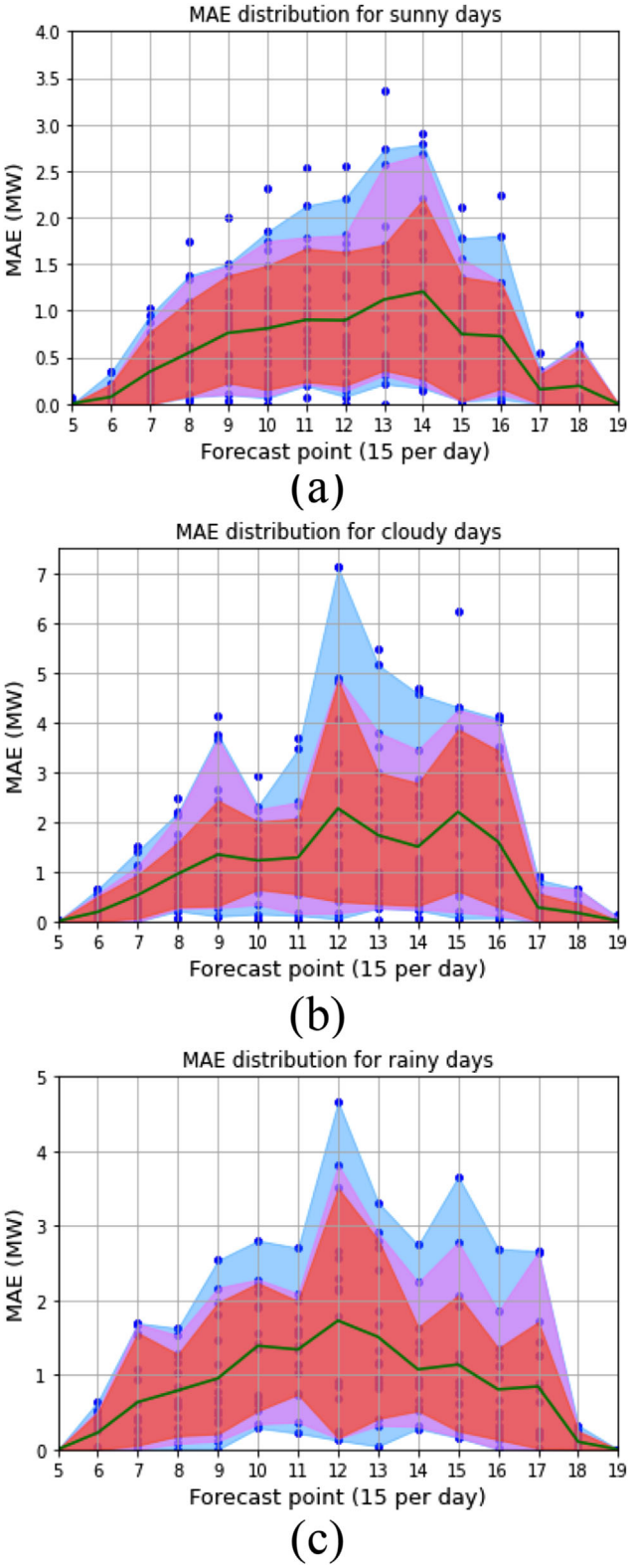

FIGURE 14 Confidence interval for hourly MAE: (a) sunny day, (b) cloudy day, (c) rainy day

TABLE 4 The average prediction performance of different models

Model	MAE	MAPE (%)	RMSE (%)	Training time(s)	Testtime(s)
CAE GAN	**0.9215**	**16.73**	**19.87**	**35,540**	**0.249**
CNN	1.0263	18.56	21.49	5146	0.137
LSTM	1.1187	19.46	23.67	2451	0.124

The CAE GAN model is trained using the training set, and then evaluated on the validation set by calculating the validation set error. Parameters are then turned accordingly. The performance of the CAE GAN model according to 10-fold cross validation is shown in Figure 15. It can be seen that the forecasting model performs consistently through validation and testing phases.

5.4 | PV power forecasting compared with popular deep learning models

To further verify the superiority of the developed model, a comparison between the developed hybrid method and other base reference models, that is, CNN and LSTM, is conducted. The base popular forecasting models are selected as reviewed in Section 2, and the comparison results are summarized in Table 4.

It can be seen from Table 4 that

1. Compared with the temporal correlation of variables extracted by LSTM, the spatial correlation of variables extracted through CNN has greater advantages to deal with PV time series involving multiple input variables. This indicates that the CAE GAN model can represent more complex non-linear relationships in regression and predict better than common neural networks such as CNN and LSTM.
2. For a small 25 MW PV plant, day-ahead PV forecast error is generally large. A slight improvement in the forecasting accuracy could be a significant impact to the whole system. The developed CAE GAN model has the highest precision, and LSTM performs worst. Computation time of LSTM is the shortest while CAE GAN has the longest one. Although the computation time of deep learning models highly depends on parameters such as batch size and learning rate, the complicated computation process is the fundamental reason for the long computation time.

The computation time includes data processing, data loading, training and testing. The reason why the hybrid method takes much longer to compute is due to the increased complexity of the model training. The CAE increases the convolutional computation of the model significantly. Since the training process can be done offline meaning we can train the models in advance. For daily operation, the testing/prediction phase is fast (in seconds), and CAE GAN is able to obtain the most accurate prediction with a well-trained model.

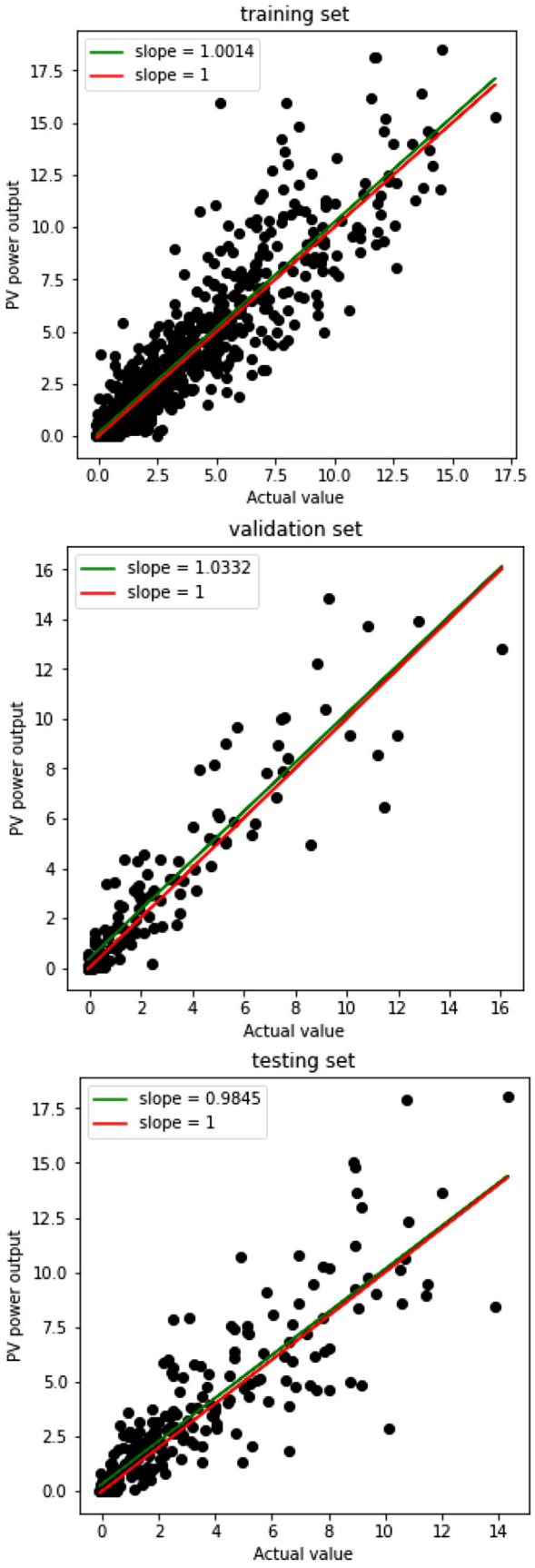

FIGURE 15 Performance of the CAE GAN model for rainy days with cross validation

TABLE 5 The forecasting performance of four models under different weather types

Weather type	Model	MAE, MW	MAPE	RMSE
Sunny day	**CAE GAN**	**0.6610**	**7.23**	**8.62**
	CNN GAN	0.7170	7.85	9.30
	FC GAN	0.6736	7.37	8.76
	LSTM GAN	0.7408	8.60	10.58
Cloudy day	**CAE GAN**	**1.1194**	**15.31**	**18.58**
	CNN GAN	1.1755	16.08	18.94
	FC GAN	1.1447	15.65	18.81
	LSTM GAN	1.2365	18.13	22.02
Rainy day	**CAE GAN**	**0.9990**	**33.09**	**38.64**
	CNN GAN	1.1680	38.68	46.98
	FC GAN	1.0805	35.79	42.44
	LSTM GAN	0.9856	34.08	41.19
Overall	**CAE GAN**	**0.9215**	**16.73**	**19.87**
	CNN GAN	1.0053	18.63	22.31
	FC GAN	0.9559	17.58	20.95
	LSTM GAN	0.9927	18.56	22.55

5.5 | PV power forecasting accuracy compared with other GAN-based models

To validate advantages of the CAE GAN, forecasting accuracies of the other three GAN-based models: CNN GAN, FC GAN and LSTM GAN are tested and compared. Forecasting errors of each weather types are summarized in Table 5.

It can be seen from Table 5 that FC GAN outperforms CNN GAN and LSTM GAN. Meanwhile, the error of CNN GAN is smaller than the prediction error produced by LSTM GAN, and this result is similar to the results of CNN vs. LSTM in Table 4, confirming that compared with the temporal correlation of variables extracted by LSTM, the spatial correlation of variables extracted through convolutions by CNN has greater advantages to deal with the PV time series involving multiple input variables. We can know that the PV power forecasting has a strong correlation not only with adjacent values, but also with distant values of input data.

The developed CAE GAN model has the best performance with small errors on different weather types and the smallest overall errors (average MAE of 0.9215, average MAPE of 16.73% and average RMSE of 19.87%) among four models. The better performance of the CAE GAN model can be explained by the stronger feature extraction ability of the CAE method. It can maintain robustness when deepening the network depth and extracting deeper features than CNN. The global skip connections between multiple layers can extract lower-frequency effective features from deeper layers for predicting the trend component of PV power and preserve some effective high-frequency features from shallow layers for predicting the detailed volatility component, which is difficult to be predicted accurately.

6 | CONCLUSIONS

PV power forecasting highly affects the power system scheduling and operation. In this paper, a hybrid day-ahead PV power forecasting method based on GAN combined with CAE is developed. A CAE-based generator for GAN is utilized for PV power forecasting. With the ability of feature enhancement of CAE and adaptive loss of GAN, this hybrid method can extract deep non-linear correlation between input and output data and improve forecasting accuracy. In contrast with the existing GAN-based models, it has a strong feature extraction ability from input data with the CAE. Testing results based on datasets from a Chinese PV station in Jiangsu province show that the developed method has higher forecasting accuracy than FC GAN, CNN GAN and other base forecasting methods as reviewed in Section 2. The developed new approach thus represents an effective and valid way to forecast day-ahead PV power generation.

The developed model makes contribution to improve the PV forecasting accuracy, and there are still challenges with the hybrid method in the PV forecasting field. (1) In the future work, we would like to consider the low prediction accuracy of cloudy and rainy days, new clustering methods for more detailed weather types are necessary. (2) As the accuracy of PV power forecasting is closely related to the accuracy of NWP, improving the accuracy of NWP is also an issue that needs further research.

NOMENCLATURE

Abbreviations

AE	autoencoder
CAE	convolutional autoencoder
CNN	convolutional neural networks
DBN	deep belief network
DHI	diffuse horizontal irradiance
DNI	direct normal irradiance
FC	fully connected neural network
GAN	generative adversarial network
GHI	global horizontal irradiance
GTI	global tilted irradiance
LSTM	long-short term memory
MAE	mean absolute error
MAPE	mean absolute percentage error
PCA	principal component analysis
PV	photovoltaic
RMSE	root mean square error
SOM	self-organizing map
TEMP	temperature
VMD	variant mode decomposition
WD	wind direction
WS	wind speed

AUTHOR CONTRIBUTIONS

xueping pan: Conceptualization; Data curation; Formal analysis; Funding acquisition; Investigation; Methodology; Resources; Supervision; Validation; Visualization; Writing – original draft. Jieyang zhou: Formal analysis; Software; Validation; Writing – original draft; Writing – review & editing. xiaorong sun: Conceptualization; Supervision; Writing – original draft; Writing – review & editing. yang cao: Conceptualization; Data curation; Formal analysis; Investigation; Methodology; Resources; Software; Validation; Visualization; Writing – original draft. xiaomei cheng: Supervision; Writing – original draft; Writing – review & editing. Hossein Farahmand: Supervision; Writing – original draft; Writing – review & editing.

ACKNOWLEDGEMENTS

The work was supported by the national key research and development program of China (No. 2019YFE0105200).

CONFLICT OF INTEREST

Any COI to declare?: No

DATA AVAILABILITY STATEMENT

Research data are not shared. Research data are not shared. cd_value_code=text

ORCID

Xueping Pan https://orcid.org/0000-0001-9756-8089
Hossein Farahmand https://orcid.org/0000-0003-1125-8296

REFERENCES

1. Das, U.K., Tey, K.S., Seyedmahmoudian, M., et al.: Forecasting of photovoltaic power generation and model optimization: A review. Renewable Sustainable Energy Rev. 81, 912–928 (2018)
2. National Energy Administration. National electric power industry statistics from. January to March (2021) http://www.nea.gov.cn/2021-05/20/c_139958706.htm
3. Hosseinian Yengejeh, H., Shahnia, F., Islam, S.M.: Impact of distributed rooftop photovoltaic systems on short-circuit faults in the supplying low voltage networks. Electric Power Components and Systems 45(20), 2257–2274 (2017)
4. Antonanzas, J., Osorio, N., Escobar, R., et al.: Review of photovoltaic power forecasting. Sol. Energy 136, 78–111 (2016)
5. Ogliari, E., Dolara, A., Manzolini, G., et al.: Physical and hybrid methods comparison for the day ahead PV output power forecast. Renewable Energy 113, 11–21 (2017)
6. Başaran, K., Bozyiğit, F., Siano, P., et al.: Systematic literature review of photovoltaic output power forecasting. IET Renewable Power Gener. 14(19), 3961–3973 (2021)
7. Ahmed, R., Sreeram, V., Mishra, Y., et al.: A review and evaluation of the state-of-the-art in PV solar power forecasting: Techniques and optimization. Renewable Sustainable Energy Rev. 124 (2020)
8. Wang, G., Su, Y., Shu, L.: One-day-ahead daily power forecasting of photovoltaic systems based on partial functional linear regression models. Renewable Energy 96, 469–478 (2016)
9. Ferbar Tratar, L., Strmčnik, E.: The comparison of Holt–Winters method and multiple regression method: A case study. Energy 109, 266–276 (2016)
10. Yang, D., Dong, Z.: Operational photovoltaics power forecasting using seasonal time series ensemble. Sol. Energy 166, 529–541 (2018)
11. Cadenas, E., Rivera, W., Campos-Amezcua, R., et al.: Wind speed prediction using a univariate ARIMA model and a multivariate NARX model. Energies 9(2), 109 (2016)
12. El-Baz, W., Tzscheutschler, P., Wagner, U.: Day-ahead probabilistic PV generation forecast for buildings energy management systems. Sol. Energy 171, 478–490 (2018)
13. Ayodele, T.R., Ogunjuyigbe, A.S.O., Amedu, A., et al.: Prediction of global solar irradiation using hybridized k-means and support vector regression algorithms. Renewable Energy Focus 29, 78–93 (2019)
14. Chen, C., Duan, S., Cai, T., et al.: Online 24-h solar power forecasting based on weather type classification using artificial neural network. Sol. Energy 85(11), 2856–2870 (2011)
15. Fu, X., Li, S.: Control of single-phase grid-connected converters with LCL filters using recurrent neural network and conventional control methods. IEEE Trans. Power Electron. 31(7), 5354–5364 (2016)
16. Wang, K., Qi, X., Liu, H.: A comparison of day-ahead photovoltaic power forecasting models based on deep learning neural network. Appl. Energy 251, 113315 (2019)
17. Almonacid, F., Rus, C., Hontoria, L., et al.: Characterisation of PV CIS module by artificial neural networks. A comparative study with other methods. Renewable Energy 35(5), 973–980 (2010)
18. Hussain, S., Alalili, A.: A hybrid solar radiation modeling approach using wavelet multiresolution analysis and artificial neural networks. Appl. Energy 208, 540–550 (2017)
19. Srivastava, S., Lessmann, S.: A comparative study of LSTM neural networks in forecasting day-ahead global horizontal irradiance with satellite data. Sol. Energy 162, 232–247 (2018)
20. Sun, Y., Venugopal, V., Brandt, A.R.: Short-term solar power forecast with deep learning: Exploring optimal input and output configuration. Sol. Energy 188, 730–741 (2019)
21. Wang, H., Lei, Z., Zhang, X., et al.: A review of deep learning for renewable energy forecasting. Energy Convers. Manage. 198, 111799 (2019)
22. Chang, G.W., Lu, H.J.: Integrating gray data preprocessor and deep belief network for day-ahead PV power output forecast. IEEE Trans. Sustainable Energy 11(1), 185–194 (2020)
23. Wang, H., Yi, H., Peng, J., et al.: Deterministic and probabilistic forecasting of photovoltaic power based on deep convolutional neural network. Energy Convers. Manage. 153, 409–422 (2017)
24. Jahangir, H., Tayarani, H., Baghali, S., et al.: A novel electricity price forecasting approach based on dimension reduction strategy and rough artificial neural networks. IEEE Trans. Ind. Inform. 16(4), 2369–2381 (2020)
25. Fu, Y., Chai, H., Zhen, Z., et al.: Sky image prediction model based on convolutional auto-encoder for minutely solar PV power forecasting. IEEE Trans. Ind. Appl. 57(4), 3272–3281 (2021)
26. Du, L., Zhang, L., Wang, X.: Generative adversarial framework-based one-day-ahead forecasting method of photovoltaic power output. IET Gener. Transm. Distrib. 14(19), 4234–4245 (2020)
27. Wang, F., Xuan, Z., Zhen, Z., et al.: A day-ahead PV power forecasting method based on LSTM-RNN model and time correlation modification under partial daily pattern prediction framework. Energy Convers. Manage. 212, 112766 (2020)
28. Huang, X., Li, Q., Tai, Y., et al.: Hybrid deep neural model for hourly solar irradiance forecasting. Renewable Energy 171, 1041–1060 (2021)
29. Agga, A., Abbou, A., Labbadi, M., et al.: Short-term self consumption PV plant power production forecasts based on hybrid CNN-LSTM, ConvLSTM models. Renewable Energy 177, 101–112 (2021)
30. Qu, J., Qian, Z., Pei, Y.: Day-ahead hourly photovoltaic power forecasting using attention-based CNN-LSTM neural network embedded with multiple relevant and target variables prediction pattern. Energy 232, 120996 (2021)
31. Drozdzal, M., Vorontsov, E., Chartrand, G., et al.: The importance of skip connections in biomedical image segmentation. Deep Learning and Data Labeling for Medical Applications. Springer, Cham, pp. 179–187 (2016)
32. Wang, F., Zhang, Z., Liu, C., et al.: Generative adversarial networks and convolutional neural networks based weather classification model for day ahead short-term photovoltaic power forecasting. Energy Convers. Manage. 181, 443–462 (2019)

33. Wang, K., Qi, X., Liu, H.: Photovoltaic power forecasting based LSTM-convolutional network. Energy 189, 116225 (2019)
34. Sun, S., Wang, S., Zhang, G., et al.: A decomposition-clustering-ensemble learning approach for solar radiation fore-casting. Sol. Energy 163, 189–199 (2018)
35. Kohonen, T., Oja, E., Simula, O., et al.: Engineering applications of the self-organizing map. Proc. IEEE 84(10), 1358–1384 (1996)
36. Yang, H.T., Huang, C.M., Huang, Y.C., et al.: A weather-based hybrid method for 1-day ahead hourly forecasting of PV power output. IEEE Trans. Sustainable Energy 5(3), 917–926 (2014)
37. China Meteorological Administration, Public Meteorological Service-Weather Graphic Symbols. China Meteorological Administration, Beijing, GB/T22164-2008 (2008)
38. Liu, L., Zhao, Y., Chang, D., et al.: Prediction of short-term PV power output and uncertainty analysis. Appl. Energy 228, 700–711 (2018)
39. Lecun, Y., Bottou, L., Bengio, Y., et al.: Gradient-based learning applied to document recognition. Proc. IEEE 86, 2278–2324 (1998)
40. Reed, S., Akata, Z., Yan, X., et al.: Generative adversarial text to image synthesis. In: International Conference on Machine Learning. PMLR, pp. 1060–1069 (2016)
41. Isola, P., Zhu, J.Y., Zhou, T., et al.: Image-to-image translation with conditional adversarial networks. In Proceedings of the IEEE Conference on Computer Vision and Pattern Recognition, pp. 1125–1134 (2017)

How to cite this article: Pan, X., Zhou, J., Sun, X., Cao, Y., Cheng, X., Farahmand, H.: A hybrid method for day-ahead photovoltaic power forecasting based on generative adversarial network combined with convolutional autoencoder. IET Renew. Power Gener. 1–15 (2022). https://doi.org/10.1049/rpg2.12619